Effects of Curvature on Flexible Bragg Grating in Off-Axis Core: Theory and Experiment

Francesco Anelli, Andrea Annunziato, Mike Godfrey, Antonella Maria Loconsole, Christopher Holmes, and Francesco Prudenzano, *Member, IEEE*

***Abstract*—A high curvature flexible Bragg grating, in planar technology, is designed, fabricated and experimentally characterized by employing silica glass. The curvature sensing mechanism for slightly off-axis core is theoretically explained and experimentally demonstrated. The electromagnetic behavior of the proposed sensor is investigated through conformal mapping, modal analysis, and coupled-mode theory. The experimental measurement reveals different sensitivities to positive and negative curvatures. The reflection spectrum of the planar Bragg grating sensor and the relationship between its resonant wavelengths and the curvature is measured for a large curvature range up to $1/R = \pm 33\ \mathrm{m}^{-1}$. The interest toward off-axis core on planar flexible platform for curvature monitoring is due to the lateral stiffness and low Young's modulus of the substrate.**

***Index Terms*—Bragg sensor, curvature, electromagnetic analysis, gratings, optical fiber devices.**

I. Introduction

OVER the last decade, research on curvature sensors has spread due to wide plethora of important applications, including structural health monitoring, kinematic motion detection and minimally invasive surgery for medical purposes, soft robotic systems, shape change in the aerospace field [1], [2], [3], [4], [5], [6], [7]. Interest in the development of flexible photonic devices has been increasing over time. Both organic and inorganic materials used to fabricate devices that can be curved, twisted, or stretched preserving the mechanical and optical performances have been proposed [8], [9], [10]. In particular, the development of flexible photonic structures and devices using ultrathin glasses, which are mechanically flexible, has provided a new opportunity in addition to the use of polymer-based materials [11]. Optical sensors are suitable for curvature measurements because of their key features such as light weight, dimensions, electromagnetic interference immunity, harsh environments operability, nontoxic, and high sensitivity [1], [12], [13]. The maximum curvature depends on the thickness of the glass and the presence of surface defects, which are related to the fabrication process [9].

Various one-dimensional curvature sensors with different operative principles have been proposed, including Bragg gratings in off-axis core [1], [14], eccentric Bragg gratings [15], [16], tilted Bragg gratings [17], [18], long period gratings [19], [20], [21], [22], and in-line interferometers [23], [24], [25]. Generally, a trade-off between complexity and sensitivity is required. The interferometric scheme benefits from higher sensitivity, but the fabrication cost and complexity could not fully meet the requirements for mass use [1], [2]. Long period gratings have some drawbacks for some specific applications. As example, the broad resonance that limits the sensor accuracy and their length results in deformation over only a fraction of the sensor when subjected to a sharp, localized curvature [14], [26], [27]. Bragg gratings can be alternative candidates for curvature sensing thanks to fabrication process maturity [1], [23].

Multidimensional curvature monitoring is spreading and multicore fibers play an important role in this context [2], [28], [29], [30], [31], [32]. Three non-aligned cores, off-axis with respect to the curvature, each of which comprising a Bragg grating, have been exploited to this aim [33], and a redundant number of cores increases the measurement reliability [29]. The overall performance of the shape change monitoring depends on the strain measurements of each Bragg grating [31]. Therefore, an in-depth study on the sensor response for slightly off-axis core position, i.e., near the "dead-zone" where small curvature strains are induced, is required.

In this paper, an accurate modeling of the curvature effect on the reflection spectrum for a few-mode, off-axis core, flexible silica planar Bragg grating is reported. The obtained results are in agreement with the experiment. A discussion on the longitudinal strain experienced by the Bragg grating explains the measured characteristics. The authors underline that, due to the curvature, the optical mode coupling within the Bragg grating is affected by the shift of the electromagnetic field profile of

Manuscript received 9 November 2022; revised 9 January 2023; accepted 17 January 2023. Date of publication 20 January 2023; date of current version 2 May 2023. This work was supported in part by Project H2020-ICT-37-2020, "Photonic Accurate and Portable Sensor Systems Exploiting Photo-Acoustic and Photo-Thermal Based Spectroscopy for Real-Time Outdoor Air Pollution Monitoring – PASSEPARTOUT" under Grant 101016956, in part by Project PON R&I 2014-2020, "New Satellites Generation components – NSG" under Grant ARS01_01215, in part by Project MIUR, PNR 2015-2020, "Agricolture Green & Digital – AGREED" under Grant ARS01_00254, and in part by the Roll-2-Roll (R2R) manufacture of multilayer planar optics under Grant EP/V053213/1. *(Corresponding author: Francesco Prudenzano.)*

Francesco Anelli, Andrea Annunziato, Antonella Maria Loconsole, and Francesco Prudenzano are with the Department of Electrical and Information Engineering, Politecnico di Bari, 70125 Bari, Italy (e-mail: francesco.anelli@poliba.it; andrea.annunziato@poliba.it; antonellamaria.loconsole@poliba.it; francesco.prudenzano@poliba.it).

Mike Godfrey is with the School of Engineering University of Southampton, Southampton SO17 1BJ, U.K. (e-mail: mrg1g16@soton.ac.uk).

Christopher Holmes is with the Optoelectronics Research Centre, University of Southampton, Southampton SO17 1BJ, U.K. (e-mail: christopher.holmes@southampton.ac.uk).

Color versions of one or more figures in this article are available at https://doi.org/10.1109/JLT.2023.3238427.

Digital Object Identifier 10.1109/JLT.2023.3238427

the propagating modes toward the region with higher refractive index. This aspect, for slightly off-axis core configuration, is essential and has to be considered in writing coupled mode theory (CMT) equations for the modelling of Bragg grating. In particular, a planar Bragg grating inscribed in a slightly off-axis core, which supports few-mode propagation, has been considered and a high curvature sensor has been designed, fabricated, and tested. The ultra-thin planar sensor consists of three doped silica layers, fabricated through flame hydrolysis deposition on a sacrificial silicon wafer. The grating is written in the central layer, making use of direct UV writing. For the first time, to the best of our knowledge, this kind of sensor is exploited for high curvature measurement. The ultra-thin platform allows to reduce the stress at surface and, thus, the possibility to extend the limited curvature measurement range of cylindrical optical fibers [20], [22], [34], [35], [36], without the use of soft materials [1], [37]. The proposed flexible planar sensors, with an off-axis core, also overcomes the limit of cylindrical optical fibers, which require that the orientation with respect to the curvature direction is guaranteed for an efficient one-dimensional curvature sensing.

The paper is organized as follows. Section I reports the introduction; Section II, the theory and simulation approach; Section III, the sensor design, fabrication, and spectrum measurement; Section IV, the comparison between numerical and experimental results; Section V, the prospects, and conclusion.

II. Theory and Simulation Approach

Generally, Bragg grating sensors written in standard optical fibers are practically not sensitive to curvature. In case of non-symmetrical configurations (e.g., off-axis core), the spectral properties of the Bragg grating are affected by curvature more significantly. The curvature induces a stress distribution within an optical waveguide, a variation of its refractive index distribution (due to the stress-optic effects) and a shift of the electromagnetic mode field profile. All these effects cause a change in the interaction between the optical modes coupled by the Bragg grating. The interaction between the propagating modes can be analyzed via the well-known CMT and via conformal mapping, briefly recalled in the following.

By considering the conformal mapping method, a curved optical waveguide, with a cross-sectional refractive index distribution n can be mapped into a straight one. For a large curvature radius R with respect to sensor size, the equivalent straight optical waveguide is characterized by a modified cross-sectional refractive index distribution n_s [27]:

$$n_s = n\left(1 + Cx_{proj}\right) \tag{1}$$

$C = 1/R$ is the curvature and $x_{proj} = rcos(\theta)$ is the projection of each point of the optical waveguide over the plane perpendicular to the neutral plane (see Fig. 1(a)). By convention, we refer to positive (negative) curvature C when the center of curvature O lies in the negative (positive) semi-axis x, see Fig. 1(a).

In addition, the modified cross-sectional refractive index distribution n_s is affected by strain components ($\varepsilon_x = \varepsilon_y = -\nu\varepsilon_z$, $\varepsilon_z = Cx_{proj}$, where ν is the Poisson's ratio) along the three principal axes induced by the curvature C. Indeed, these

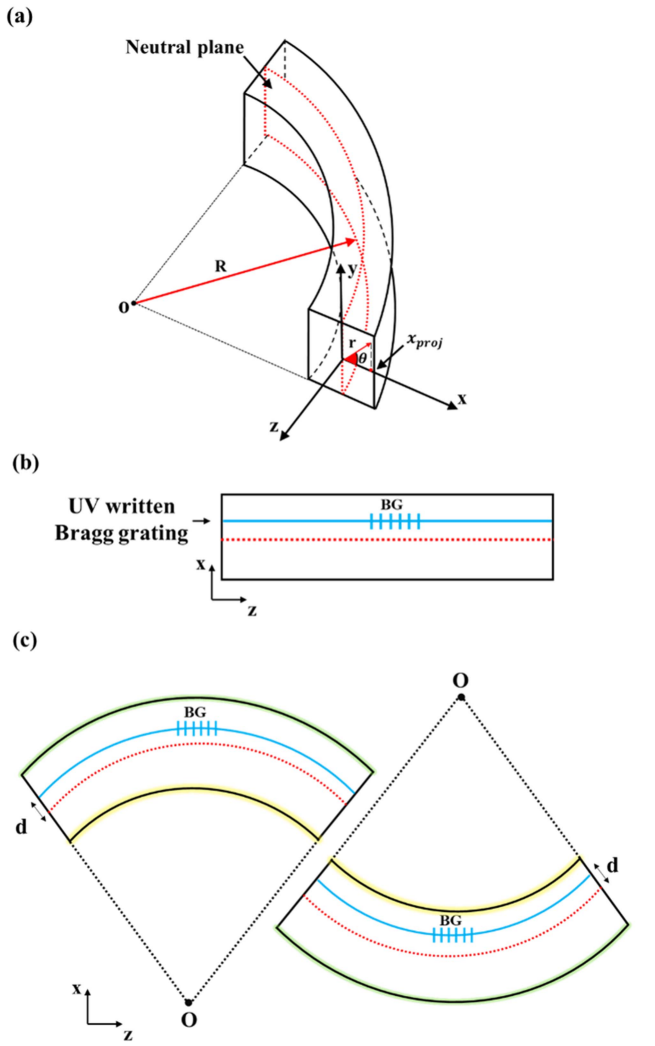

Fig. 1. (a) 3D-sketch of a curved waveguide. (b) 2D-sketch of the straight optical waveguide. (c) 2D-sketch of the curved optical waveguide with positive (left) and negative (right) curvature C (green colored line for tensile strain, yellow colored line for compressive strain).

strains, alter the cross-sectional refractive index distribution n which needs to be evaluated by considering the stress-optic relations [27]:

$$n = n_0 + \Delta n = n_0 - \left(\frac{n_0^3}{2}\right)\left(p_{12} - vp_{12} - vp_{11}\right) Cx_{proj} \tag{2}$$

where n_0 is the refractive index distribution of the optical waveguide without curvature, p_{11} and p_{12} the components of the photo-elastic tensor [38]. For silica, $p_{11} = 0.121$, $p_{12} = 0.27$, $v = 0.16$ [39], [40].

Fig. 1(b) shows the 2D-sketch of the straight optical waveguide, in blue colored the off-axis UV written Bragg grating. In Fig. 1(c), the 2D-sketches of the curved optical waveguide for positive and negative curvature C are reported. In Fig. 1(c), the strain component along the z-axis ε_z introduces a compression (yellow colored line) along the inner half with respect to the neutral plane, and tension (blue colored line) along the outer half

of the device. The neutral plane (red dotted line) is not affected by strain and the refractive index distribution n does not change. These tensile and compressive strains modify the cross-sectional refractive index n according to the relation (2). The value of the refractive index increases with respect to n_0 in the outer half of the device, while decreases in the inner half [24]. The modified refractive index distribution n_s is employed to calculate the electromagnetic fields distributions of the fundamental and high order propagating modes, via 2D-finite element method (2D-FEM). The transversal electromagnetic field distributions are calculated both for the straight and curved waveguide. As a result, the transversal electromagnetic field profile of the propagating modes, within the curved optical waveguide, shifts toward the region with higher refractive index [40]. The CMT can be used to explain the relationship between the spectral response of the Bragg grating and the curvature C. Before solving the coupled mode equations, the transversal coupling coefficients $K^t(z)$ are calculated for all the propagating modes travelling in the positive $+z$ and negative $-z$ direction [40]:

$$K_{\pm}^{t}(z) = \frac{w}{4} \iint_{core} \Delta\epsilon(x,y,z)\, E_{+}^{t}(x,y,z)\, \overline{E_{-}^{t}}(x,y,z)\, dxdy \tag{3}$$

where w is the angular frequency of the propagating light and $\Delta\epsilon(x,y,z)$ is the dielectric perturbation which is dependent on curvature C, and related to the imposed refractive index modulation [41]; $E^t(x,y,z)$ is the transversal electromagnetic field profile depending on curvature C. The CMT longitudinal coupling coefficients $K^z(z)$, are two orders of magnitude smaller than transversal ones $K^t(z)$, therefore they are neglected. Finally, the CMT equations can be solved.

In addition, if the Bragg grating is located outside the neutral plane, the nominal Bragg grating pitch Λ_0 changes as $\Lambda = \Lambda_0\,(1+\varepsilon_z)$. Generally, for ε_z calculation, x_{proj} corresponds to the distance between the center of the Bragg grating and the neutral plane, defined as core offset d (see Fig. 1(c)) [42], [43], [44]. This approximation is no longer true when the distance d is comparable or smaller than the core size of the optical waveguide. In this case, the shift of the electromagnetic field profile of the propagating modes toward the region with higher refractive index cannot be neglected in the mode coupling calculation [37], [42], [43], [44], [45].

The simulation approach employed for the design is summarized as follows: i) conformal mapping in order to describe the curved waveguide with an equivalent one, ii) 2D-finite element method (2D-FEM) to compute the electromagnetic mode analysis of the equivalent waveguide, iii) calculation of the coupling coefficient $K_{\pm}^{t}(z)$ [46], iv) implementation of the CMT as a boundary value problem to evaluate counter-propagating modes powers. The procedure is repeated for each wavelength λ in the range of interest, with a defined wavelength step $\Delta\lambda$, and for each curvature value C. The implemented approach is complete, accurate and applicable to any type of multimode optical waveguide. Approximated investigations consider Gaussian beam with a closed form equation [37] or adopt simplified equations without the implementation of CMT [16], [27], [34], [37].

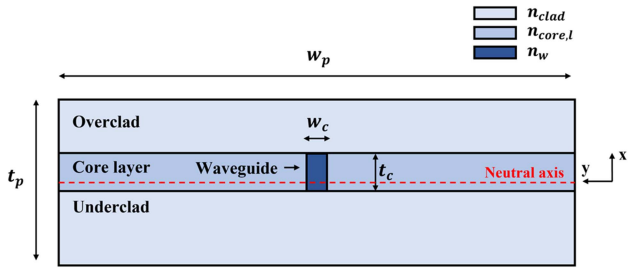

Fig. 2. Sketch of the designed planar Bragg grating sensor. The waveguide in which the grating is inscribed (blue colored) is written in the central core layer and it is slightly off-axis with respect to the neutral axis.

III. Design and Fabrication of the Sensor

A. Sensor Design

A design is performed with the aim of investigating the response of a curvature sensor for slightly off-axis core position. The planar technology is chosen to avoid the orientation problem typical of unidirectional curvature sensing with cylindrical optical fiber. The geometrical and physical parameters are feasible with the available technology, consisting of flame hydrolysis deposition and physical machining [47]. In order to make more evident the effect of electromagnetic modes profile shift, a few-mode waveguide is chosen. Fig. 2 reports a not to scale sketch of the designed planar Bragg grating sensor. The core thickness $t_c = 19.5\ \mu$m is larger than the core width $w_c = 14.5\ \mu$m, leading to great electromagnetic modes shift along the x axis, see Fig. 2. The other geometrical parameters are width $w_p = 1$ mm, thickness $t_p = 57\ \mu$m, core offset $d = 1.2\ \mu$m. The thickness t_p is thin enough to reduce surface stresses and thick enough to avoid evanescent field exposure.

The underclad and overclad silica glass regions have identical composition with a refractive index $n_{clad} = 1.444$ at the wavelength $\lambda = 1570$ nm. Step-index profile is assumed for both the core layer and the waveguide. In particular, the refractive index of the core layer is $n_{core,l} = 1.4633$ and of the waveguide is $n_w = 1.4713$ at the wavelength $\lambda = 1570$ nm. The wavelength dispersion is modelled via proper Sellmeier equation [48]. The effective refractive indices and electromagnetic field profiles of all the propagating modes are simulated via FEM and considered in CMT equations. The effective refractive index of the fundamental mode, simulated via FEM, is $n_{eff} = 1.4712$ at the wavelength $\lambda = 1570$ nm when the sensor is not subjected to curvature C.

The designed uniform Bragg grating has a sinusoidal modulation with an amplitude $\Delta n_{BG} = 2 \times 10^{-4}$ and a length $L = 12$ mm. The nominal grating period Λ_0, when the planar sensor is not subjected to curvature C, is $\Lambda_0 = 0.534\ \mu$m. This value is designed to obtain the mode matching between the forward and backward fundamental mode around the wavelength $\lambda = 1570$ nm.

As described in Section II, the curvature C determines a shift of the electromagnetic field of the propagating modes towards the waveguide region with higher refractive index. As

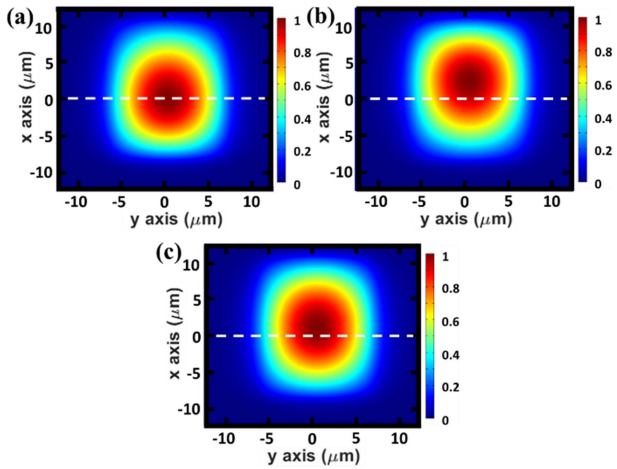

Fig. 3. Norm of the electric field E of the fundamental mode for: (a) Curvature $C = -33\ \mathrm{m}^{-1}$, (b) Curvature $C = 33\ \mathrm{m}^{-1}$, (c) Curvature $C = 0\ \mathrm{m}^{-1}$.

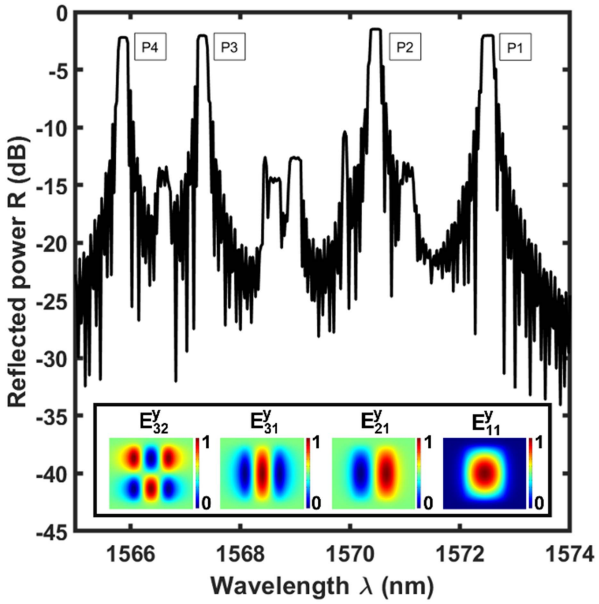

Fig. 4. Simulated reflection spectrum of the planar Bragg grating sensor when no curvature C is applied; length of the Bragg grating $L = 1.2$ mm, refractive index modulation of the Bragg grating $\Delta n_{BG} = 2 \times 10^{-4}$. In the inset, the y component of the electric field for y polarized modes E^y_{11}, E^y_{21}, E^y_{31}, E^y_{32}.

an example, Fig. 3 reports the shift of electric field norm E of the fundamental mode for curvature $C = [0\ \mathrm{m}^{-1},\ \pm 33\ \mathrm{m}^{-1}]$.

The simulation is carried out in the wavelength range λ from 1565 nm to 1574 nm with a wavelength step $\Delta\lambda = 5\ pm$.

The simulated reflection spectrum when the planar Bragg grating is not curved is reported in Fig. 4. The UV written waveguide is few-mode. The spatial modes are classified as E_{lm} modes, where l and m depends on the number of maxima and minima of the electric field distributions along the y axis and x axis of the rectangular core [49].

Four propagating modes interacts with the Bragg grating inducing multiple resonant wavelengths, marked as P1, P2, P3, P4, corresponding to the spatial modes E_{11}, E_{21}, E_{31}, E_{32}, respectively. For the sake of simplicity, only one of the almost degenerate orthogonal polarizations E^y_{lm} is reported in the inset of Fig. 4.

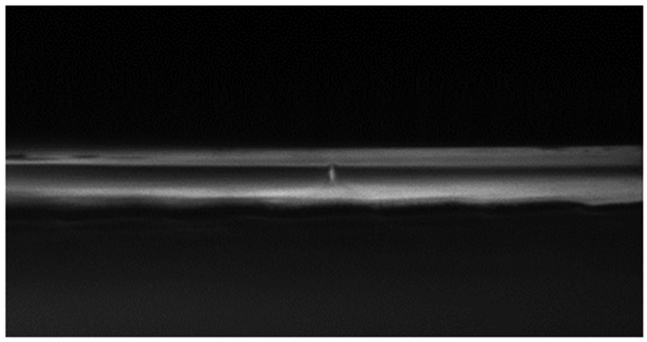

Fig. 5. Enlargement of the cross section of the planar Bragg sensor captured via CCD camera.

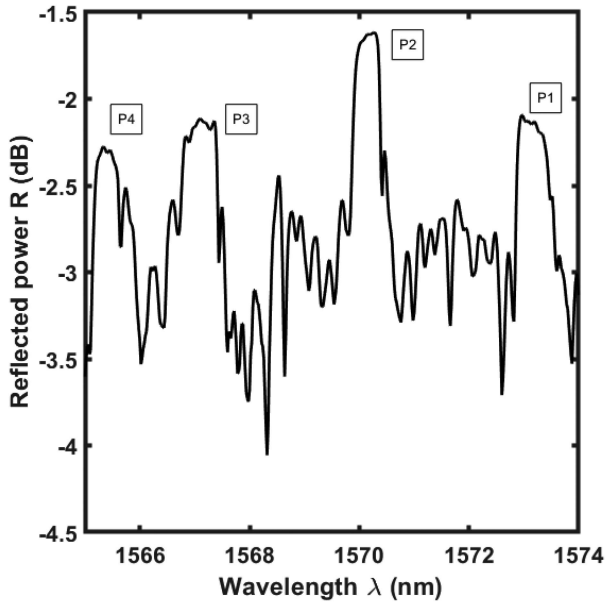

Fig. 6. Measured reflection spectrum of the planar Bragg grating sensor when no curvature C is applied; length of the Bragg grating $L = 1.2$ mm, refractive index modulation of the Bragg grating $\Delta n_{BG} = 2 \times 10^{-4}$.

B. Sensor Fabrication and Spectrum Measurement

Flame Hydrolysis Deposition (FHD) is made upon a sacrificial p-doped [1 0 0] silicon wafer with diameter $d_{Si} = 152$ mm. Three doped silica layers: overclad, core and underclad are deposited and the silicon is later removed through physical machining, leaving a flexible glass substrate with a nominal thickness $t_p = 57\ \mu$m. Fig. 5 shows an image of the cross-section of the planar sensor captured through a CCD camera.

The overclad, core and underclad are clearly distinguishable. Underclad does not possess a constant thickness because of the removal of the silicon wafer through physical machining.

Direct UV writing is employed to inscribe the few-mode waveguide and the uniform Bragg grating in the core layer.

The planar Bragg grating reflection spectrum, measured through optical spectrum analyzer, is reported in Fig. 6; the

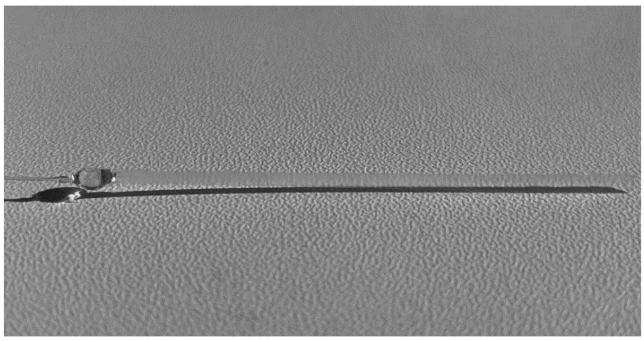

Fig. 7. Planar Bragg sensor butt-coupled to a cylindrical optical fiber through UV curable adhesive.

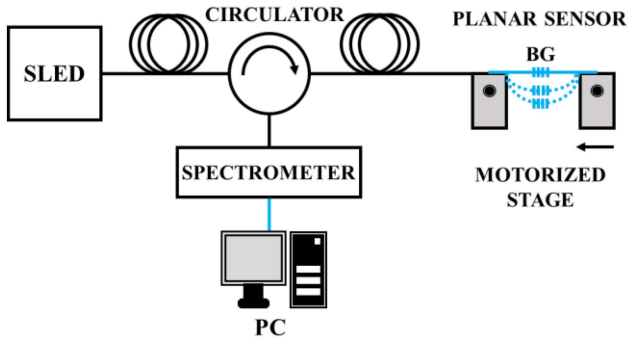

Fig. 8. Experimental set-up adopted for the curvature measurement of the planar Bragg grating.

planar sensor is butt-coupled to a cylindrical optical fiber through UV curable adhesive, as shown in Fig. 7. Four resonant wavelengths are apparent in Fig. 6 due to the few guided modes. The different reflected powers depend mainly on i) the mode power distribution in the few-mode waveguide; ii) the corresponding coupling coefficients $K_{\pm}^{t}(z)$. Furthermore, an unwanted Bragg grating chirping is evident, induced by UV writing. The measured resonant peaks are in good agreement with the simulated ones.

IV. Curvature Effect

Different values of curvature C are considered taking into account positive and negative curvature directions. For comparison between simulation and experiment, the considered curvature values are: $C = 0\ \mathrm{m}^{-1}$, $\pm 8.5\ \mathrm{m}^{-1}$, $\pm 16\ \mathrm{m}^{-1}$, $\pm 23\ \mathrm{m}^{-1}$, $\pm 28\ \mathrm{m}^{-1}$, $\pm 33\ \mathrm{m}^{-1}$. In order to characterize the sensor response to curvature C, it is important to vanish the influence of cross-sensitivities induced by temperature and/or spurious strain not directly related to curvature C. To this aim, the measurements are carried out in a temperature-controlled environment. A mount and a motorized stage are employed to perform curvature C measurement and particular attention is paid to avoid that the clamping could affect the planar Bragg grating spectral characteristics. Furthermore, the use of mount and motorized stage suppresses any unintentional twisting effect.

In addition, to compensate any effects of temperature, the Bragg wavelength shift $\Delta\lambda_B$ is measured as the difference between the resonance peak when the sensor is subjected to curvature C and the resonance peak when the sensor is not curved. To perform high resolution measurement the Bayspec FBGA optical spectrometer is employed instead of the optical spectrum analyzer. The spectrometer guarantees a minimum detectable wavelength change $r = \pm 1\ pm$ and allows the detection of peaks P3 and P4. A sketch of the adopted experimental set-up is reported in Fig. 8.

The measured Bragg wavelength shift $\Delta\lambda_B$ (black squares) as a function of curvature C are reported in Fig. 9 for peak P3 and in Fig. 10 for peak P4 showing good agreement with numerical results. Both the characteristics of Figs. 9 and 10 show an almost linear characteristic for positive curvature C values.

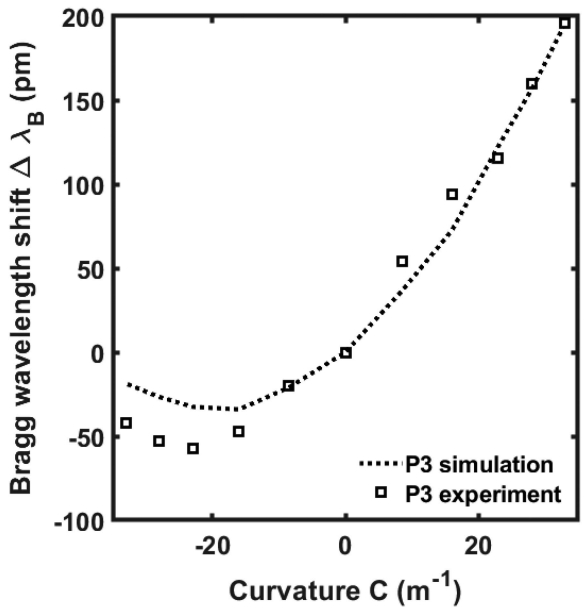

Fig. 9. Simulated (dotted line) and measured (square markers) Bragg wavelength shift $\Delta\lambda_B$ of the resonance peak P3 for curvature $C = 0\,\mathrm{m}^{-1}, \pm 8.5\,\mathrm{m}^{-1}, \pm 16\ \mathrm{m}^{-1}, \pm 23\ \mathrm{m}^{-1}, \pm 28\ \mathrm{m}^{-1}, \pm 33\ \mathrm{m}^{-1}$.

In particular, for positive values of curvature C, the electromagnetic field shifts toward the outer half of the planar Bragg grating sensor. It is mainly subjected to tensile strain ϵ_z, which linearly increases with curvature C. The linearized sensitivity for positive values of curvature C is $S_{P3}^{+} = 5.9\ pm/\mathrm{m}^{-1}$ for the peak P3 and $S_{P4}^{+} = 5.2\,pm/\mathrm{m}^{-1}$ for the peak P4. The reason for the dissimilar values of linearized sensitivity S^{+} is due to the difference in the effective refractive indices between the straight and curved planar Bragg grating sensor for each mode. The difference in the effective refractive indices for peak P3 is greater than for peak P4, causing the Bragg wavelength shift of the peak P3 to be larger than that of the peak P4. This is directly influenced by the mode profile being considered. Decreasing the value of curvature C, the electromagnetic field shifts in the opposite direction toward the centre of the planar sensor. In particular, when the curvature C is slightly negative, the electromagnetic field is affected by the compressive strain ϵ_z effect. By further decreasing the curvature C, the electromagnetic field intercepts the neutral plane, where no strains along the principal axes occur,

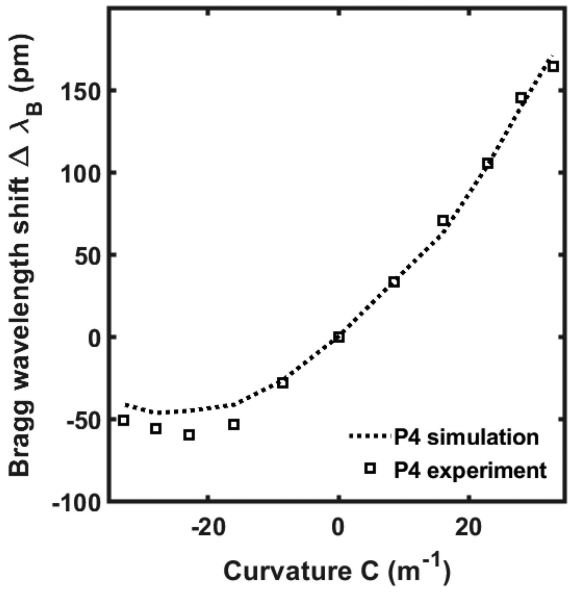

Fig. 10. Simulated (dotted line) and measured (square markers) Bragg wavelength shift $\Delta\lambda_B$ of the resonance peak P4 for curvature $C = 0\,\mathrm{m}^{-1}$, $\pm 8.5\,\mathrm{m}^{-1}$, $\pm 16\,\mathrm{m}^{-1}$, $\pm 23\,\mathrm{m}^{-1}$, $\pm 28\,\mathrm{m}^{-1}$, $\pm 33\,\mathrm{m}^{-1}$.

and the sensitivity becomes zero, around $C = -23\,\mathrm{m}^{-1}$. As the curvature C becomes more negative, the electromagnetic field marginally extends beyond the neutral plane and tensile strain ϵ_z is experienced. Therefore, the combined effect of cross-sectional refractive index change and tensile strain ϵ_z on the grating period Λ, leads to a reversal of the slope. To summarize, for positive values of curvature C, the electromagnetic field shifts progressively toward the outer half of the device, where increasingly higher tensile strain ϵ_z occurs; for negative values of curvature C, the electromagnetic field shifts from the inner half, where the compressive strain ϵ_z occurs, toward the outer half of the device, where there is a tensile strain ϵ_z, see Fig. 1(c).

V. Conclusion

For the first time, a high curvature sensor based on ultra-thin flexible silica planar Bragg grating is proposed, designed, and experimentally characterized. The implementation of CMT-based code explains the resonant wavelengths shift for different curvatures. The experimental results agree with simulation and are reported for high curvature up to $\pm 33\,\mathrm{m}^{-1}$, showing an excellent mechanical robustness also with respect to the optical fiber solution. The device exhibits different sensitivities when positive and negative curvatures are applied. This is theoretically explained with a discussion on the longitudinal strain to which the Bragg grating is subjected. This concept finds applications also in curvature direction and radius sensing in multicore optical fibers. Future sensors and reconstruction algorithm can be engineered taking into account the demonstrated principle, leading to a better shape reconstruction. Lastly, the possibility to customize the geometry and the waveguides position, the absence of orientation problems typical of cylindrical optical fiber makes the adopted planar photonic platform attractive for new generation photonic sensing devices.

References

[1] J. Ge, A. E. James, L. Xu, Y. Chen, K.-W. Kwok, and M. P. Fok, "Bidirectional soft silicone curvature sensor based on off-centered embedded fiber Bragg grating," *IEEE Photon. Technol. Lett.*, vol. 28, no. 20, pp. 2237–2240, Oct. 2016.

[2] D. Budnicki et al., "All-fiber vector bending sensor based on a multicore fiber with asymmetric air-hole structure," *J. Light. Technol.*, vol. 38, no. 23, pp. 6685–6690, Dec. 2020.

[3] H. Wu, L. Liang, H. Wang, S. Dai, Q. Xu, and R. Dong, "Design and measurement of a dual FBG high-precision shape sensor for wing shape reconstruction," *Sensors*, vol. 22, no. 1, 2022, Art. no. 168.

[4] M. Rosenberger, H. Pauer, M. Girschikofsky, H. Woern, B. Schmauss, and R. Hellmann, "Flexible polymer shape sensor based on planar waveguide Bragg gratings," *IEEE Photon. Technol. Lett.*, vol. 28, no. 17, pp. 1898–1901, Sep. 2016.

[5] F. Attivissimo, A. Di Nisio, A. M. L. Lanzolla, and M. A. Ragolia, "Analysis of position estimation techniquesin a surgical EM tracking system," *IEEE Sensors J.*, vol. 21, no. 13, pp. 14389–14396, Jul. 2021.

[6] G. Brunetti, G. Marocco, A. Di Benedetto, A. Giorgio, M. N. Armenise, and C. Ciminelli, "Design of a large bandwidth 2×2 interferometric switching cell based on a sub-wavelength grating," *J. Opt.*, vol. 23, no. 8, 2021, Art. no. 085801.

[7] E. Bertolesi, M. Fagone, T. Rotunno, E. Grande, and G. Milani, "Experimental characterization of the textile-to-mortar bond through distributed optical sensors," *Construction Building Mater.*, vol. 326, Apr. 2022, Art. no. 126640.

[8] G. C. Righini, J. Krzak, A. Lukowiak, G. Macrelli, S. Varas, and M. Ferrari, "From flexible electronics to flexible photonics: A brief overview," *Opt. Mater.*, vol. 115, 2021, Art. no. 111011.

[9] G. Macrelli, A. K. Varshneya, and J. C. Mauro, "Ultra-thin glass as a substrate for flexible photonics," *Opt. Mater.*, vol. 106, 2020, Art. no. 109994.

[10] A. Lukowiak, S. Jiang, and M. Ferrari, "Foreword," *Opt. Mater.*, vol. 129, 2022, Art. no. 112555.

[11] T. N. L. Tran et al., "Rare-earth activated SnO2 photoluminescent thin films on flexible glass: Synthesis, deposition and characterization," *Opt. Mater.*, vol. 124, 2022, Art. no. 111978.

[12] M. De Carlo, F. De Leonardis, R. A. Soref, and V. M. N. Passaro, "Design of an exceptional-surface-enhanced silicon-on-insulator optical accelerometer," *J. Light. Technol.*, vol. 39, no. 18, pp. 5954–5961, 2021.

[13] R. Pashaie and M. Vahedi, "Simultaneous measurement of temperature and strain of a fixed composite cantilever using a π-PSFBG sensor," *Opt. Quantum Electron.*, vol. 54, no. 2, pp. 1–3, 2022.

[14] D. Feng, X. Qiao, and J. Albert, "Off-axis ultraviolet-written fiber Bragg gratings for directional bending measurements," *Opt. Lett.*, vol. 41, no. 6, pp. 1201–1204, 2016.

[15] X. Chen, C. Zhang, D. J. Webb, K. Kalli, and G.-D. Peng, "Highly sensitive bend sensor based on Bragg grating in eccentric core polymer fiber," *IEEE Photon. Technol. Lett.*, vol. 22, no. 11, pp. 850–852, Jun. 2010.

[16] W. Bao, Q. Rong, F. Chen, and X. Qiao, "All-fiber 3D vector displacement (bending) sensor based on an eccentric FBG," *Opt. Exp.*, vol. 26, no. 7, pp. 8619–8627, 2018.

[17] L. Shao, L. Xiong, C. Chen, A. Laronche, and J. Albert, "Directional bend sensor based on re-grown tilted fiber Bragg grating," *J. Lightw. Technol.*, vol. 28, no. 18, pp. 2681–2687, 2010.

[18] Y. Jin, C. Chan, X. Dong, and Y. Zhang, "Temperature-independent bending sensor with tilted fiber Bragg grating interacting with multimode fiber," *Opt. Commun.*, vol. 282, no. 19, pp. 3905–3907, 2009.

[19] Y. P. Wang and Y. J. Rao, "A novel long period fiber grating sensor measuring curvature and determining bend-direction simultaneously," *IEEE Sensors J.*, vol. 5, no. 5, pp. 839–843, Oct. 2005.

[20] X. Xu et al., "A vector bending sensor based on a core-offset long period fiber grating induced by an arc-discharge," *IEEE Sensors J.*, vol. 21, no. 21, pp. 24129–24133, Nov. 2021.

[21] H. Jung et al., "Bending and strain sensitivities in a helicoidal long-period fiber gratings," *IEEE Photon. Technol. Lett.*, vol. 21, no. 17, pp. 1232–1234, Sep. 2009.

[22] X. Zhong et al., "Bending characteristics of a long-period fiber grating in a hollow eccentric optical fiber," *Appl. Opt.*, vol. 54, no. 26, pp. 7879–7883, 2015.

[23] Y. Tian et al., "Directional bending sensor based on a dual side-hole fiber Mach–Zehnder interferometer," *IEEE Photon. Technol. Lett.*, vol. 30, no. 4, pp. 375–378, Feb. 2018.

[24] Y. Wu et al., "Highly sensitive curvature sensor based on asymmetrical twin core fiber and multimode fiber," *Opt. Laser Technol.*, vol. 92, pp. 74–79, 2017.

[25] A. Sun and Z. Wu, "Multimode interference in single mode–multimode FBG for simultaneous measurement of strain and bending," *IEEE Sensors J.*, vol. 15, no. 6, pp. 3390–3394, Jun. 2015.
[26] Q. Rong, X. Qiao, H. Yang, K. S. Lim, and H. Ahmad, "Fiber Bragg grating inscription in a thin-core fiber for displacement measurement," *IEEE Photon. Technol. Lett.*, vol. 27, no. 10, pp. 1108–1111, May 2015.
[27] A. Taghipour, A. Rostami, M. Bahrami, H. Baghban, and M. Dolatyari, "Comparative study between LPFG-and FBG-based bending sensors," *Opt. Commun.*, vol. 312, pp. 99–105, 2014.
[28] M. Hou et al., "Two-dimensional vector bending sensor based on seven-core fiber Bragg gratings," *Opt. Exp.*, vol. 26, no. 18, pp. 23770–23781, 2018.
[29] F. Khan, A. Denasi, D. Barrera, J. Madrigal, S. Sales, and S. Misra, "Multi-core optical fibers with Bragg gratings as shape sensor for flexible medical instruments," *IEEE Sensors J.*, vol. 19, no. 14, pp. 5878–5884, Jul. 2019.
[30] D. Zheng, J. Madrigal, H. Chen, D. Barrera, and S. Sales, "Multicore fiber-Bragg-grating-based directional curvature sensor interrogated by a broadband source with a sinusoidal spectrum," *Opt. Lett.*, vol. 42, no. 18, pp. 3710–3713, 2017.
[31] I. Floris, S. Sales, P. A. Calderón, and J. M. Adam, "Measurement uncertainty of multicore optical fiber sensors used to sense curvature and bending direction," *Measurement*, vol. 132, pp. 35–46, 2019.
[32] S. L. Jantzen et al., "Individual inscription of spectrally multiplexed Bragg gratings in optical multicore fibers using small spot direct UV writing," *Opt. Exp.*, vol. 28, pp. 21300–21309, 2020.
[33] G. M. H. Flockhart, W. N. MacPherson, J. S. Barton, J. D. C. Jones, L. Zhang, and I. Bennion, "Two-axis bend measurement with Bragg gratings in multicore optical fiber," *Opt. Lett.*, vol. 28, no. 6, pp. 387–389, 2003.
[34] J. H. Osório et al., "Bragg gratings in surface-core fibers: Refractive index and directional curvature sensing," *Opt. Fiber Technol.*, vol. 34, pp. 86–90, 2017.
[35] X. Hu, X. Chen, C. Liu, P. Mégret, and C. Caucheteur, "D-shaped polymer optical fiber Bragg grating for bend sensing," in *Proc. OSA Adv. Photon. Congr.*, Boston, MA, USA, 2015, Paper SeS2B.5.
[36] K. Yang et al., "Femtosecond laser inscription of fiber Bragg grating in twin-core few-mode fiber for directional bend sensing," *J. Light. Technol.*, vol. 35, no. 21, pp. 4670–4676, Nov. 2017.
[37] M. Jang, J. S. Kim, S. H. Um, S. Yang, and J. Kim, "Ultra-high curvature sensors for multi-bend structures using fiber Bragg gratings," *Opt. Exp.*, vol. 27, no. 3, pp. 2074–2084, 2019.
[38] R. T. Schermer and J. H. Cole, "Improved bend loss formula verified for optical fiber by simulation and experiment," *IEEE J. Quantum Electron.*, vol. 43, no. 10, pp. 899–909, Oct. 2007.
[39] A. M. Smith, "Birefringence induced by bends and twists in single-mode optical fiber," *Appl. Opt.*, vol. 19, pp. 2606–2611, 1980.
[40] C. Holmes, M. Godfrey, D. J. Bull, and J. Dulieu-Barton, "Real-time through-thickness and in-plane strain measurement in carbon fibre reinforced polymer composites using planar optical Bragg gratings," *Opt. Lasers Eng.*, vol. 133, 2020, Art. no. 106111.
[41] W. Zhang, X. Lei, W. Chen, H. Xu, and A. Wang, "Modeling of spectral changes in bent fiber Bragg gratings," *Opt. Lett.*, vol. 40, no. 14, pp. 3260–3263, 2015.
[42] C. Liu, X. Yang, F. Laurell, and M. Fokine, "Fabrication of a widely tunable fiber Bragg grating filter using fused deposition modeling 3D printing," *Opt. Mater. Exp.*, vol. 9, no. 11, pp. 4409–4417, 2019.
[43] J. Kong, X. Ouyang, A. Zhou, H. Yu, and L. Yuan, "Pure directional bending measurement with a fiber Bragg grating at the connection joint of eccentric-core and single-mode fibers," *J. Light. Technol.*, vol. 34, no. 14, pp. 3288–3292, Jul. 2016.
[44] C. L. Tien, T. C. Cheng, L. C. Chen, G. R. Lin, and W. F. Liu, "Simultaneous measurement of bending curvature and axial stress using D-shaped fiber Bragg gratings," in *Proc. Int. Conf. Opt. Instrum. Technol.: Adv. Sensor Technol. Appl.*, 2009, pp. 387–392.
[45] H. S. Phing, J. Ali, R. A. Rahman, and B. A. Tahir, "Fiber Bragg grating modeling, simulation and characteristics with different grating lengths," *Mal. J. Fundam. Appl. Sci.*, vol. 3, no. 2, pp. 167–175, Dec. 2007.
[46] H. Haus, W. Huang, S. Kawakami, and N. Whitaker, "Coupled-mode theory of optical waveguides," *J. Light. Technol.*, vol. 5, no. 1, pp. 16–23, Jan. 1987.
[47] C. Holmes, M. Godfrey, P. L. Mennea, S. Zahertar, and J. Barton, "Flexible photonics in low stiffness doped silica for use in fibre reinforced polymer composite materials," *Opt. Mater.*, vol. 134, Dec. 2022, Art. no. 113133.
[48] I. H. Malitson, "Interspecimen comparison of the refractive index of fused silica," *J. Opt. Soc. Amer.*, vol. 55, no. 10, pp. 1205–1208, 1965.
[49] Y. Wu and K. S. Chiang, "Mode-selective coupling between few-mode fibers and buried channel waveguides," *Opt. Exp.*, vol. 24, no. 16, pp. 30108–30123, 2016.

Francesco Anelli received the M.Sc. degree in 2021 in electronic engineering (*cum laude*) from Politecnico di Bari, Bari, Italy, where he is currently working toward the Ph.D. degree in electrical and information engineering. His research interests include the modeling and the characterization of optical fiber grating sensors and fused optical fiber components.

Andrea Annunziato received the M.Sc. degree in electronic engineering (*cum laude*) from Politecnico di Bari, Bari, Italy, in 2020. He is currently working toward the Ph.D. degree in engineering and aerospace sciences. His research interests include the modeling and the characterization of fiber lasers, optical fiber sensors for aerospace applications, and Mid-IR optical devices.

Mike Godfrey is currently working toward the Ph.D. degree in engineering with the University of Southampton, Southampton, U.K. His work ranges from the development of novel orthopaedic implants through to optical sensing and composites. He has worked on various optical strain sensing techniques. His research interests started with tribology, before turning to optical sensing for composite structural health monitoring in collaboration with the Optoelectronics Research Centre.

Antonella Maria Loconsole received the M.Sc. and Ph.D. degrees from Politecnico di Bari, Bari, Italy, in 2019 and 2022, respectively. Her research interests include SIW antennas, microwave applicators for medical applications, and optical fiber lasers, amplifiers, and sensors.

Christopher Holmes is currently a Royal Society Industry Fellow with GE Aviation and Principal Enterprise Fellow with Optoelectronics Research Centre, University of Southampton, Southampton, U.K. He is also the Principal Investigator with U.K. Engineering and Physical Science Research Council (EPSRC) Grant EP/V053213/1 developing new flexible silica planar optics, captured in this work. He is the Chair of Optica (formally Optical Society of America) Technical Group, on Optical Fabrication and Testing and an Associate Editor for *IET Science, Measurement and Technology*.

Francesco Prudenzano (Member, IEEE) has been a Full Professor of electromagnetic fields with Politecnico di Bari, Bari, Italy, and the Head of Microwave and Optical Engineering Group, Department of Electrical and Information Engineering, Politecnico di Bari, since 2018. From 2016 to 2015, he was the Vice Chair and the Chair of SIOF from 2017 to 2018, Italian Society of Optics and Photonics (Italian branch of EOS - European Optical Society). From 2018 to 2020, he was the Vice Chair of CoRiFI-The Italian Coordination of Innovation and Research on Photonic. Since 2021, he has been the Member of Politecnico di Bari Board Directors. From 2016 to 2021, he was the Chair of Teacher Council of the first level degree in electronic and communication engineering, and has been the Chair of the second level degree in Communication Engineering since 2021. He has coauthored more than 450 publications, many of which got published in journals and international conferences, lectures, and invited papers. He is involved in several national and international research and cooperation projects, also with the role of Scientific Coordinator. He was the Project Leader and co-Leader within COST MP0702 and MP1401, actions in the field of photonics. He was also the Chair of national and international conferences.

Open Access funding provided by 'Politecnico di Bari' within the CRUI CARE Agreement